Characterization of Photodamage to *Escherichia coli* in Optical Traps

Keir C. Neuman,*#‖ Edmund H. Chadd,# Grace F. Liou,§ Keren Bergman,¶‖ and Steven M. Block*#‖
Departments of *Physics, #Molecular Biology, §Chemical Engineering, and ¶Electrical Engineering, and ‖Princeton Materials Institute, Princeton University, Princeton, New Jersey 08544 USA

ABSTRACT Optical tweezers (infrared laser-based optical traps) have emerged as a powerful tool in molecular and cell biology. However, their usefulness has been limited, particularly in vivo, by the potential for damage to specimens resulting from the trapping laser. Relatively little is known about the origin of this phenomenon. Here we employed a wavelength-tunable optical trap in which the microscope objective transmission was fully characterized throughout the near infrared, in conjunction with a sensitive, rotating bacterial cell assay. Single cells of *Escherichia coli* were tethered to a glass coverslip by means of a single flagellum: such cells rotate at rates proportional to their transmembrane proton potential (Manson et al., 1980. *J. Mol. Biol.* 138:541–561). Monitoring the rotation rates of cells subjected to laser illumination permits a rapid and quantitative measure of their metabolic state. Employing this assay, we characterized photodamage throughout the near-infrared region favored for optical trapping (790–1064 nm). The action spectrum for photodamage exhibits minima at 830 and 970 nm, and maxima at 870 and 930 nm. Damage was reduced to background levels under anaerobic conditions, implicating oxygen in the photodamage pathway. The intensity dependence for photodamage was linear, supporting a single-photon process. These findings may help guide the selection of lasers and experimental protocols best suited for optical trapping work.

INTRODUCTION

"Optical tweezers," or optical traps, provide a unique means of manipulating and controlling biological objects (Svoboda and Block, 1994). Since the first demonstration of optical trapping by Ashkin (1978, 1986), a host of applications have arisen in biology, both in vivo and in vitro. A drawback of optical trapping has been the damage induced by the intense trapping light. In practice, such damage limits the exposure time for trapped specimens and has proved to be a significant problem for some optical trapping studies, particularly those in vivo. Indeed, Ashkin first encountered this problem and coined the colorful term "opticution" to describe the laser-induced death of specimens (Ashkin and Dziedzic, 1989). The potential for damage is readily appreciated by computing the light level at the diffraction-limited focus of a typical trapping laser: for a power of just 100 mW, the intensity is 10^7 W/cm^2, with an associated flux of 10^{26} photons/s·cm^2 (traps used in cell biology are generally based on lasers producing from 25 mW to 2 W in the specimen plane). Proposed mechanisms for photodamage include transient local heating (Liu et al., 1996), two-photon absorption (Berns, 1976; König et al., 1995, 1996a; Liu et al., 1996), and photochemical processes leading to the creation of reactive chemical species (Calmettes and Berns, 1983; Block, 1990; Svoboda and Block, 1994; Liu et al., 1996).

Some practical progress has been made toward decreasing photodamage in optical trapping systems, primarily through the choice of trapping lasers with wavelengths in the near-infrared region (Ashkin et al., 1987). This corresponds to a waveband that is comparatively transparent to biological material, situated between the absorption bands of many biological chromophores in the visible, and the increasing absorption of water toward longer wavelengths (Svoboda and Block, 1994). The most common source used in optical traps is the continuous-wave (CW) diode-pumped Nd:YAG laser (1064 nm) or its close relatives, Nd:YLF (1047 nm) and Nd:YVO_4 (1064 nm). These represent the most economical choices for achieving the requisite power (1–10 W) and output stability. But other sources suitable for optical trapping exist. Recent years have seen the emergence of high-intensity, single-mode diode lasers, available in the wavelength region from 700-1500 nm, with powers up to ~1 W. Diode lasers possess exceptional amplitude stability and are more economical than Nd-based lasers. Another option is the CW Ti:sapphire laser, which affords continuous tuning through much of the near-infrared region (700–1000 nm), along with high output power. However, it requires a separate pump source, typically suffers reduced amplitude stability, and is far and away more costly than the alternatives. For now, Nd-based lasers continue to dominate the optical trapping field, but sources at other wavelengths may represent more advantageous choices for reducing photodamage.

Berns and co-workers pioneered investigations of photodamage in optical traps, using a variety of biological assays. Their work with temperature-sensitive fluorescent dye reporters in Chinese hamster ovary (CHO) cells and lipo-

Received for publication 13 May 1999 and in final form 30 July 1999.

Address reprint requests to Dr. Steven M. Block, Department of Biological Sciences, Gilbert Building, Room 109, 371 Serra Mall, Stanford University, Stanford, CA 94305-5020. Tel.: 650-724-4046; fax: 650-723-6132; E-mail: sblock@stanford.edu.

Mr. Neuman's and Dr. Block's present address is Department of Biological Sciences, Stanford University, Stanford, CA 94305.

Ms. Liou's present address is Department of Chemical Engineering, Stanford University, Stanford, CA 94305.

0006-3495/99/11/2856/08 $2.00

somes confirmed the prediction that local heating of micron-sized specimens is negligible from a tightly focused CW laser source, thereby ruling out direct heating as a source of damage (Block, 1990; Liu et al., 1995a, 1996). Additional studies, based on assays of the rates of chromosome bridge formation in rat kangaroo cells (Vorobjev et al., 1993) or cloning efficiency in CHO cells (Liang et al., 1996), established rough action spectra for damage over portions of the near-infrared region. Following this work, additional studies, scoring either CHO cell-cloning efficiency or loss of viability in human spermatozoa, led to the suggestion that damage is generated by a two-photon process (König et al., 1995, 1996a,b; Liu et al., 1996). In addition, work with fluorescent probes demonstrated no changes in the intracellular pH of trapped cells and no detectable changes in DNA structure following CW laser illumination (as opposed to pulsed lasers, which do produce changes in acridine orange staining) (Liu et al., 1996).

While such experiments provide important clues to the photodamage process, the bioassays upon which they are based have certain intrinsic limitations. Chromosome bridge formation is largely qualitative and difficult to score. Cloning efficiency and sperm viability essentially provide a binary output (alive or dead), necessitating many measurements to gain adequate statistics. The assays are indirect, complex, and time consuming, requiring long incubation and/or growth periods, together with sensitive fluorescence-measuring capabilities. Furthermore, they do not readily lend themselves to the continuous monitoring of photodamage during experimental exposure.

To address these limitations, we employed a rotating bacterial cell assay that provides a quantitative, real-time measure of the metabolic state of the cell. The assay is based on attaching *Escherichia coli* cells to a glass coverslip by a single flagellum (Block et al., 1982, 1989). When the tethered cell turns its flagellar motor, the cell body is driven into rotation about its point of attachment, typically ~0–15 Hz, depending upon the cell size (and therefore on the load posed by viscous rotational drag). Motors of tethered cells spin at rates proportional to the transmembrane proton potential (Manson et al., 1980).

Although based on a prokaryote, this assay has some advantages over the eukaryotic systems employed previously. *E. coli* are robust and well-characterized organisms, which can be grown either aerobically or anaerobically, permitting evaluation of the role of oxygen in photodamage. Moreover, an enormous variety of mutants is available.

Using this assay, in conjunction with a broadly tunable optical trapping system, we determined the action spectrum for photodamage from 790 to 1064 nm. This spectrum shows a roughly sevenfold variation in damage across this range, with two pronounced maxima at 870 and 930 nm. The least damaging wavelength was found to be 970 nm, followed closely by 830 nm. By growing and trapping cells in the absence of oxygen (or by removing oxygen after growth with a chemical scavenging system), we tested the effect of oxygen on the lifetime of cells. There was a significant increase in lifetime under anaerobic conditions: in fact, damage was reduced to nearly background levels. Determining photodamage as a function of laser power (at two different wavelengths, 870 and 1064 nm), we found that the sensitivity of cells (defined as the reciprocal of the lifetime) was linearly related to the intensity. These results suggest that photodamage in optical traps is mediated by oxygen, and that it involves a one-photon process.

MATERIALS AND METHODS

Optics

The optical trap (schematic shown in Fig. 1) was based on three separate lasers: a Ti:sapphire ring laser tunable between 780 nm and 970 nm (model 899; Coherent, Santa Clara, CA), a MOPA diode laser at 991 nm (model 5762-A6; SDL, San Jose, CA), and a Nd:YAG laser at 1064 nm (model BL-106C; Spectra-Physics Lasers, Mountain View, CA). The Ti:sapphire laser was pumped with all lines from a large-frame argon ion laser (Innova 400; Coherent). To ensure true continuous-wave output from the Ti:sapphire laser, we incorporated an intercavity etalon (model 895; Coherent), which reduces the bandwidth and prevents temporal mode beating and partial modelocking (König et al., 1996a). The laser output was monitored in both temporal and frequency domains to check for pulses, which are indicative of temporal mode beating. Without the etalon, pulses were observed at a repetition rate of 186 MHz, corresponding to the round-trip time in the cavity. With the etalon in place, all mode beating ceased. The spatial mode of the Ti:sapphire laser and of the YAG laser was TEM_{00}, while the mode from the MOPA was slightly elliptical (ellipticity = 1.3). The output from the laser was expanded to slightly overfill the back pupil of the microscope objective (63×/1.2 numerical aperture (NA) Plan NeoFluar, water/glycerol immersion, model 461832; Carl Zeiss, Oberkochen, Germany) and brought into an inverted microscope (Diaphot TMD; Nikon, Tokyo, Japan) via the epiillumination port. The optical path

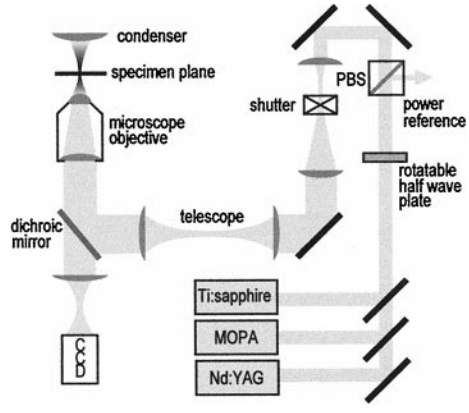

FIGURE 1 Simplified schematic of the tunable optical trap (not to scale). To cover the near-infrared spectrum, one of three separate lasers was selected: the Ti:sapphire ring laser allows continuous tuning from 790 nm to 970 nm; the MOPA laser is at 991 nm; the Nd:YAG is at 1064 nm. The laser power is controlled via a rotatable halfwave plate and polarizing beam splitter (PBS). After the polarizer, the beam is expanded to slightly overfill the back pupil of the microscope objective. In the middle of the beam expander is a computer-controlled shutter. The laser is then directed into the epiillumination path of an inverted microscope and reflected by a dichroic mirror into the microscope objective. The objective focuses the laser light to form a trap in the specimen plane and collects visible light from the condenser to form an image. The visible light passes through the dichroic mirror to a video camera (CCD).

included a computer-driven shutter (model 845; Newport Corp., Irvine, CA) controlling the laser trap. A dichroic mirror (model 635DCSPX; Chroma Technology Corp., Brattleboro, VT) in the microscope directed the laser into the objective while permitting the visible light, imaged by the objective, to pass through. Blue light artifacts induced by the microscope illumination source (50-W, 12-V DC halogen bulb) were minimized by placing a green interference filter (Nikon) in the illumination pathway.

Rotating, tethered cells were imaged on a CCD camera (model V-1056SX CCD; Video Runner, Culver City, CA). A time code generator (model TRG-50; Horita Co., Mission Viejo, CA) added a time stamp to the video signal, which was displayed on a B/W monitor (model PVM-97; Sony Corp., Montvale, NJ) and recorded by VCR (model AG-1980; Panasonic Co., Secaucus, NJ). In most cases, rotation rates of cells were simultaneously analyzed using a custom-built video cursor box placed in the video chain, which delivered a TTL pulse to a computer whenever the position of a rotating cell crossed a user-defined cursor position (Block and Berg, 1984). The same cursor box could also be used off-line with videotaped records of cells.

Microscope objective transmission calibration

To determine accurately the power delivered to the specimen plane, the transmission of the microscope objective must be characterized. Because of the high NA and short working distance of objectives used for optical trapping work, transmission cannot be measured by simply passing a beam of light through the lens and collecting it with an ordinary photodetector. Instead, the objective transmission as a function of wavelength was measured using a dual-objective technique (Misawa et al., 1991), as described by Svoboda and Block (1994). Measured transmission curves for several candidate objectives are displayed in Fig. 2.

Calibration of power in the specimen plane

The power in the specimen plane was determined by a multistep procedure. First, the microscope objective used for optical trapping was replaced by a low-NA objective with a known transmittance (20×/0.4 NA, model M-20X; Newport Corp.; transmittance determined separately). A pyroelectric optical power meter (model LM-10; Coherent) was placed in front of this objective, at (or near) the specimen position, to record the intensity of light passing through. The power at this position, P_m, is related to the power delivered to the specimen plane in an actual experiment using a high-NA objective, P_a, by $P_a = P_m \cdot T_1(\lambda)/T_2(\lambda)$, where $T_1(\lambda)$ is the measured transmission of the high-NA objective and $T_2(\lambda)$ is the measured transmission of the low-NA objective. (The entrance pupils of the low-NA objective and the high-NA objectives have the same diameter.) Next, to set the power at the specimen for any given wavelength, λ', the half-wave plate in front of the polarizing beam splitter (PBS) was adjusted to obtain a reading of $P_m = P_a \cdot T_2(\lambda')/T_1(\lambda')$ on the optical power meter. The low-NA objective was then replaced with the high-NA trapping objective. Once the power was established in this way, any drift in power could be monitored via the second PBS port and corrected during an experiment. Power measurements as just described were performed before trapping in each experiment and after each change in the wavelength.

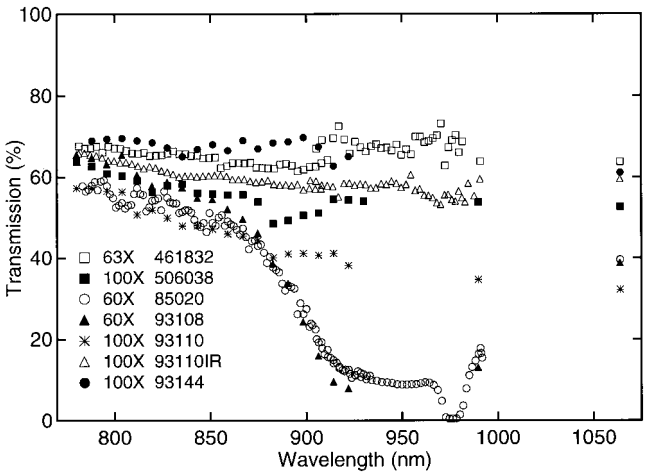

FIGURE 2 Microscope objective transmission curves. Transmission measurements were made by a dual-objective method (see Materials and Methods). Part numbers are cross-referenced in Table 1. The uncertainty associated with a measurement at any wavelength is ~5%.

Bacterial assay

We employed a tethered cell assay (Block et al., 1982, 1989) based on a strain of *E. coli* that carries two useful mutations (KAF95, a gift of Karen Fahrner, Harvard University; Berg and Turner, 1993). The first mutation is a deletion of the *cheY* gene. CheY-P protein induces clockwise rotation of the flagellar motor; in its absence, cells rotate smoothly in the counterclockwise direction (Parkinson, 1978; Parkinson et al., 1983), facilitating measurements of rotation rates. The second mutation affects the flagellar protein flagellin. In KAF95, the *fliC* gene encoding flagellin has an internal deletion leading to a nonspecific binding interaction between flagella and the negative surface charge on the coverglass (Kuwajima, 1988). Cells carrying both of these mutations spontaneously tether themselves and rotate continuously in the counterclockwise direction.

Cells of *E. coli* strain KAF95 were grown as described by Block et al. (1982), except that cultures were grown in T-broth (10 mg ml^{-1} Bacto-Tryptone, Difco Laboratories, Detroit, MI; 5 mg ml^{-1} NaCl, Sigma, St. Louis, MO), supplemented with 100 μg ml^{-1} ampicillin (Sigma) at 30°C, and the motility medium was that described by Block et al. (1983). Cells were loaded into a flow cell consisting of a coverslip attached to a microscope slide by two pieces of double-sided tape. Cells were allowed to tether for 10–15 min, after which time the flow cell was washed with 900-1200 μl of motility medium to remove untethered cells.

The experimental procedure was modified slightly to study cells under reduced oxygen tension. To ensure anaerobic conditions, mineral oil (Fisher Scientific, Pittsburgh, PA) was layered over the surface of the growth medium before incubation to prevent oxygen from entering the test tube (cells consume any residual oxygen during the early stages of growth). The entire shearing and tethering process was carried out under nitrogen inside a glove bag, and the flow cell was sealed all around with vacuum grease (Apiezon M; M&I Materials, Manchester, England) before exposure to air. In other experiments, anaerobic conditions were achieved by introducing an oxygen-scavenging system into the flow cell after tethering but before trapping (250 μg ml^{-1} glucose oxidase, 30 μg ml^{-1} catalase, 4.5 mg ml^{-1} glucose; Sigma). We estimate the time required to deplete the remaining oxygen in the flow cell under these conditions to be less than 1 s.

Tethered cells were held by the optical trap and periodically released to monitor their rotation rates (Fig. 3). In a typical experiment, once a suitably tethered cell was identified (initial frequency of 5–12 Hz), between 30 and 100 s of data was collected before the trap was turned on. Thereafter, during each successive 10-s interval, the cell was held for 8 s by the trap and then released for 2 s. The rotation rate was determined from the timing of pulses generated by the video cursor box corresponding to full rotations (above). Pulses were captured by a data acquisition board (model AT-MIO-16E-10; National Instruments, Austin, TX), using a Labview program (Labview 4; National Instruments), which was also used to control data acquisition and analyze rotation rates. Rotational data were further analyzed with Igor software (Igor Pro; Wavemetrics, Lake Oswego, OR). The data were smoothed, the start time (corresponding to when the trap was first turned on) was established, and the LD_{50} time, operationally defined as the time at which the rotation rate decreased to 50% of its initial value, was determined (see Fig. 4). Control data were obtained in a similar manner, but with cells exposed only to the microscope illumination. Experiments were performed at 25–27°C. A typical flow cell had one or two well-tethered cells per field of view (200 μm^2). After data were

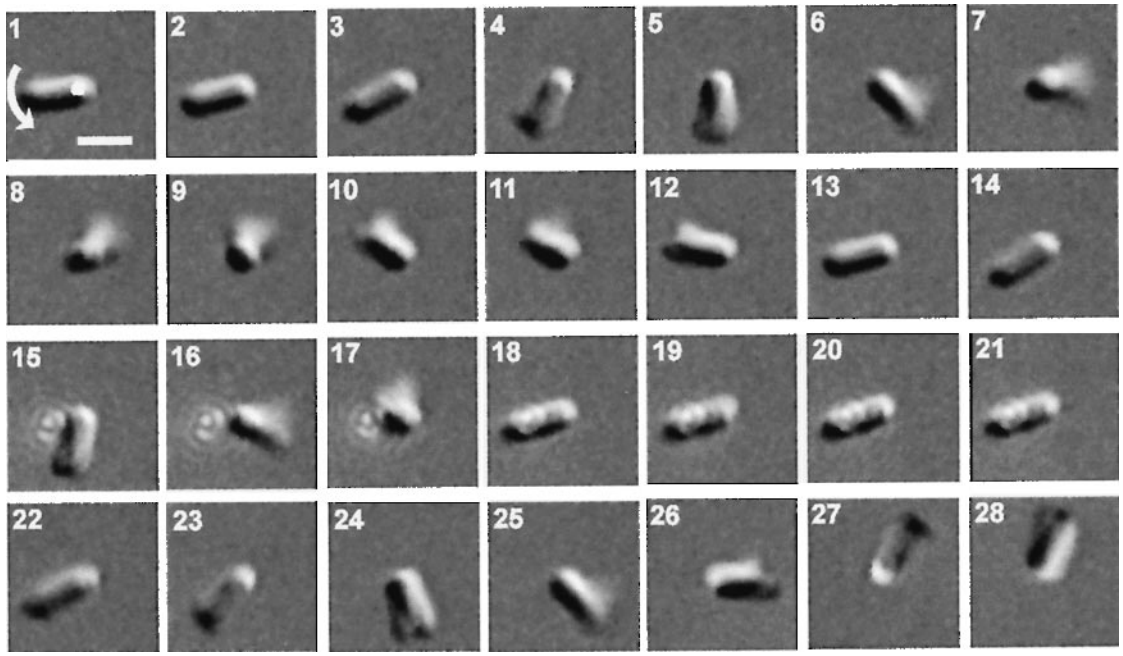

FIGURE 3 Images of a single rotating cell of *E. coli* tethered to a glass coverslip and imaged with DIC microscopy: successive video fields are displayed (time interval, 33 ms/field). The scale bar is 1 μm; the curved arrow indicates the direction of rotation, and the white dot shows the approximate center of rotation. The first 14 frames show the cell spinning freely (at ~2.5 Hz). The next 14 frames were taken with the trap on (the diffraction-limited laser focus is seen as concentric rings in frame 15). The cell rotates into, and is held by, the trap for four frames (18–21), before release (frame 22), after which it continues to rotate (frames 23–28).

acquired from a cell, the next cell was chosen at least 400 μm away from the first. No more than two flow cells were made from a single culture. To mitigate the effect of systematic variation in cell behavior from day to day, data for each point were collected from a minimum of three preparations over 2 days, with each point representing the average of 6–23 individual LD_{50} determinations. There was no correlation between initial rotation rate and LD_{50} time (correlation coefficient $r = 0.1$). We defined sensitivity as the inverse of the LD_{50} time. Data are presented as mean ± SEM.

RESULTS

Microscope objective transmission calibration

Measured transmission data for seven high-NA microscope objectives from three manufacturers are presented in Fig. 2 and Table 1. Overall transmission for the group varied from 1% to 73%. All objectives showed acceptable transmission in the short-wavelength region of the infrared spectrum (~45–65%, ~790–830 nm). Beyond 850 nm, the transmission of most Plan Apo objectives fell dramatically, in certain cases to levels unacceptable for optical trapping work. However, objectives designed primarily for fluorescence work (Plan NeoFluar, Zeiss; Plan Fluor, Nikon) or explicitly for work in the near IR (93110IR; Nikon) had improved transmission characteristics in the longer wavelength region.

Wavelength-dependent damage

Control cells exposed to light from the microscope lamp, but not from the trapping laser, had an average LD_{50} time of 3300 ± 400 s, with a corresponding sensitivity of $3.1 \times 10^{-4} \pm 0.4 \times 10^{-4}$ s^{-1}. The action spectrum (i.e., the wavelength-dependent sensitivity) for *E. coli* trapped at 100 mW of laser power (determined in the specimen plane) is presented in Fig. 5. There was a roughly sevenfold difference between the most damaging wavelength (930 nm) and the least (970 nm). A direct comparison between the photodamage spectrum measured for *E. coli* and that reported

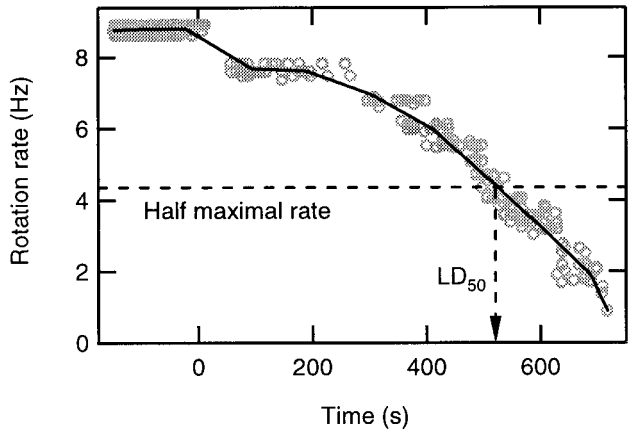

FIGURE 4 Rotation rate as a function of time for a single cell (*open gray circles*, experimental data; *solid line*, a linear spline fit to the data). The trap is turned on at $t = 0$, after which there is a gradual decrease in rotation rate. The LD_{50} is depicted on the graph as the time at which the rotation rate decreased to 50% of the initial value. The appearance of layer lines in the data is a consequence of the video detection scheme, which requires an integral number of frames.

TABLE 1 Transmission of microscope objectives, cross-referenced with Fig. 2

Part no.	Manufacturer	Magnification/tube length (mm)/numerical aperture	Type designation	Transmission (±5%) 830 nm	850 nm	990 nm	1064 nm
461832	Zeiss	63/160/1.2 water	Plan NeoFluar	66	65	64	64
506038	Leica	100/∞/1.4–0.7 oil	Plan Apo	58	56	54	53
85020	Nikon	60/160/1.4 oil	Plan Apo	54	51	17	40
93108	Nikon	60/∞/1.4 oil	Plan Apo CFI	59	54	13	39
93110	Nikon	100/∞/1.4 oil	Plan Apo CFI	50	47	35	32
93110IR	Nikon	100/∞/1.4 oil	Plan Apo IR CFI	61	60	59	59
93144	Nikon	100/∞/1.3 oil	Plan Fluor CFI	67	68	—	61

by Liang et al. (1996), based on cell cloning efficiency, is displayed in Fig. 6.

Oxygen-dependent damage

A comparison between cells trapped under either aerobic or anaerobic conditions at two different wavelengths is presented in Fig. 7. Anaerobic conditions were achieved either by growing and maintaining cells in an oxygen-free environment or by introducing an oxygen-scavenging system just before trapping. The experimental results were statistically identical in the two cases. The effect on photodamage of removing oxygen was dramatic, resulting in a three- to sixfold increase in LD_{50}. Notably, trapping lifetimes under anaerobic conditions were the same as for the controls.

Intensity dependence of photodamage

Clues to the photochemical process underlying optical damage can be gained from the study of its intensity dependence. A simplified model for photodamage takes the form $S(P) = A + BP^n$, where S is the sensitivity, A is the control sensitivity, B is the wavelength-dependent sensitivity, and P is the power. For a single photon-based process, n should be 1, while for a two-photon process, n should be 2. A double-logarithmic plot of the reduced sensitivity, S-A, as a function of power at 870 and 1064 nm is plotted in Fig. 8. Data sets for each wavelength were fit to lines. At 1064 nm, the slope was 1.14 ± 0.03 (reduced $\chi^2 = 4.2$), while at 870 nm the slope was 0.91 ± 0.06 (reduced $\chi^2 = 2.5$). Taken together, the average slope is 1.06 ± 0.07, consistent with a linear, one-photon process.

Temporal dependence of photodamage

A distinct attribute of the rotating cell assay is an ability to obtain quantitative data from a single cell in real time (Fig. 4). Averaged single-cell curves for data taken at 870 nm with 100 mW are plotted in Fig. 9. To compute this average, individual curves were first normalized by their initial rotation rates, and then the time was normalized by the measured LD_{50}. While there was considerable variation among individual curves, the average behavior displays an approximately linear decrease in rotation speed with time.

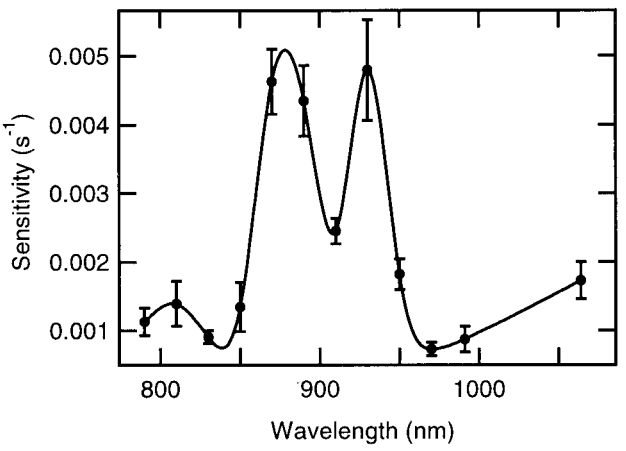

FIGURE 5 The action spectrum for *E. coli* trapped with 100 mW. Sensitivity is defined as the reciprocal of the average LD_{50}. (*solid circles*, experimental data; *solid line*, a cubic spline fit to the data). Each point represents an average of 12–23 determinations, with the errors shown (±SEM).

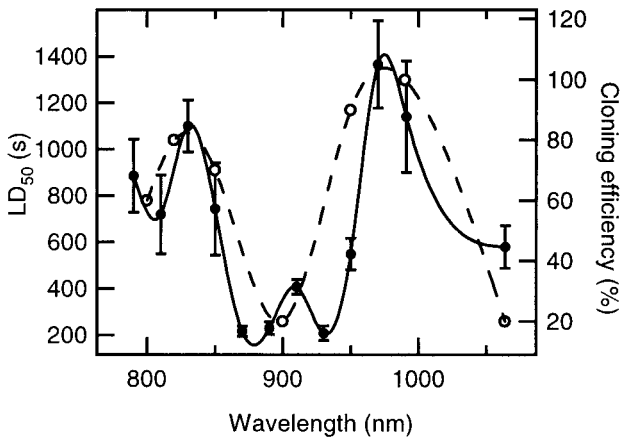

FIGURE 6 The wavelength dependence of photodamage in *E. coli* compared to CHO cells (*solid circles and solid line, left axis,* data replotted from Fig. 5 as LD_{50}; *open circles and dashed line, right axis,* cloning efficiency determined by Liang et al., 1996 (used with permission)). Lines represent cubic spline fits to the data. The cloning efficiency in CHO cells was determined after 5 min of trapping at 88 mW in the specimen plane (error bars unavailable), selected to closely match to our experimental conditions (100 mW in the specimen plane; errors are shown as ±SEM).

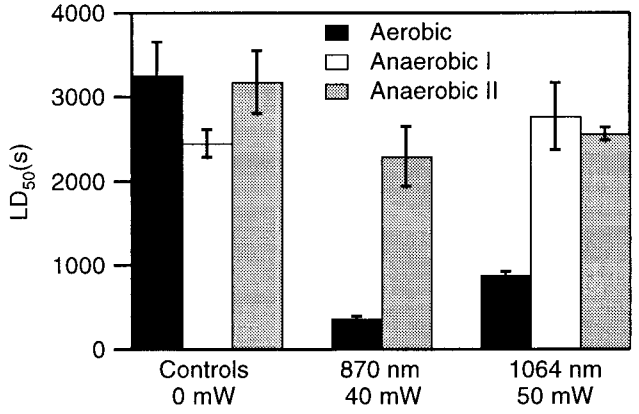

FIGURE 7 The oxygen dependence of photodamage. Comparison between *E. coli* cells trapped under aerobic and anaerobic conditions (*solid bars*, cells grown and maintained aerobically; *open bars*, cells trapped in the presence of an oxygen scavenging system; *gray bars*, cells that were grown and maintained anaerobically). Each point represents an average of 6–12 determinations, with the errors shown (± SEM).

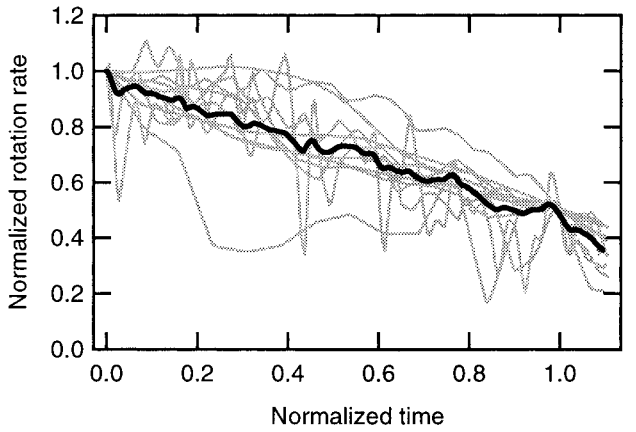

FIGURE 9 Photodamage as a function of time at 870 nm and 100-mW trapping power. *Gray lines*, normalized rotation rates versus normalized time. Rates were normalized according to their initial values, determined over an interval of ~30–100 s before the start of trapping at $t = 0$. Time was normalized according to the individual LD_{50} time determined for each cell, and typically ranged from ~200 to 300 s. *Solid line*, the unweighted average of these curves.

DISCUSSION

The prominent features exhibited by the photodamage action spectrum (Fig. 5) are not easily understood. For example, the spectrum does not bear any superficial resemblance to the absorption spectrum of suspensions of *E. coli* cells, to water absorption (Palmer and Williams, 1974), or to the absorption of molecular oxygen (Krupenie, 1972). The relatively sharp spectral features suggest that light is absorbed by one or more specific photopigments. However, our effort to match the observed spectrum with known chromophores was hampered by a dearth of spectral data for biological molecules in the near-infrared region (most published spectra do not extend beyond ~750 nm). One noteworthy characteristic is the rough similarity between the wavelength dependence of photodamage seen in *E. coli* and in CHO cells (Fig. 6). This may indicate a common basis for damage in both prokaryotic and eukaryotic systems, possibly involving a ubiquitous intracellular chromophore, and suggests that it may be possible to generalize the present results, with caveats, to other organisms.

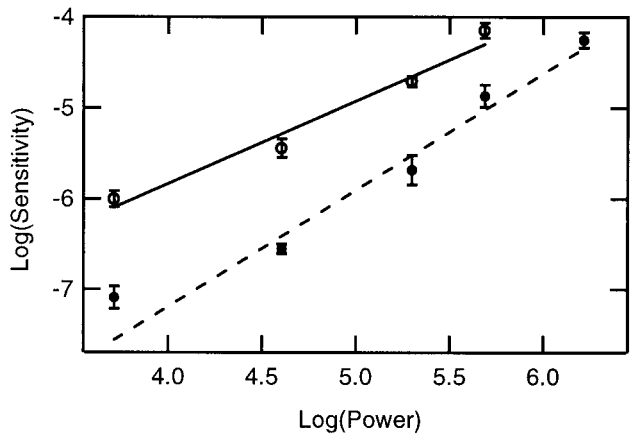

FIGURE 8 The intensity dependence of photodamage. Double logarithmic plot of the reduced sensitivity, *S-A*, versus power in the specimen plane at 870 nm (*open circles, solid line*) and at 1064 nm (*filled circles, dashed line*). The data are fit to lines, the slope of which gives the apparent order of the photodamage process. Fitted slope at 870 nm, 0.911 ± 0.06 (reduced $\chi^2 = 2.5$); slope at 1064 nm, 1.14 ± 0.03 (reduced $\chi^2 = 4.2$).

The dramatic increase in LD_{50} under anaerobic conditions (Fig. 7) implies a critical role for oxygen in the damage pathway. In its absence, trapped cells display a LD_{50} comparable to that of control cells. Whether oxygen is directly responsible, through the formation of a reactive oxygen species (the primary candidate being singlet molecular oxygen), or simply mediates the process remains to be determined.

The nearly linear relationship between sensitivity and power strongly suggests that a single-photon mechanism leads to photodamage (Fig. 8). This implies a direct absorption by some molecule (or molecules) in the infrared region, as opposed to a two-photon excitation mechanism in the visible (or UV) by unidentified fluorophores. This conclusion is at variance with previous reports implying a role for a two-photon process (König et al., 1995, 1996a; Liu et al., 1996), which were based on the finding that photodamage depended on the peak intensity, and not the average intensity, when short-pulse laser irradiation was used (pulsed lasers are not normally used for optical trapping work). However, the clearest signature for a two-photon process is a quadratic dependence of damage on laser intensity, which was not explicitly established. One possible resolution of the discrepancy may be that there are two regimes for photodamage: at the extremely high peak intensities generated by mode-locked and Q-switched lasers (GW/cm^2; König et al., 1996a), photodamage may be dominated by some two-photon process, while at the lower intensities encountered in CW optical traps (operating at MW/cm^2), the single-photon mechanism prevails. An alternative ex-

planation for the increased damage seen with pulsed lasers may be the onset of optoacoustic shock waves (Hu, 1969; Bushanam and Barnes, 1975; Patel and Tam, 1981), which are pressure waves generated from high-intensity light pulses focused into a liquid medium. The overpressures produced can amount to several atmospheres and may have deleterious effects. Optoacoustic damage has been studied in bulk tissues (Yashima et al., 1990, 1991; Lustmann et al., 1992) but not in single cells.

The ability to continuously monitor single cells in the optical trap reveals the progress of the damage process. The nearly linear decline in rotation rate displayed by Fig. 9 was found for all wavelengths and laser powers investigated. Photodamage therefore seems to be a gradual process, not a catastrophic one. A damage threshold did not appear to exist. Even at the lowest power investigated, the rotation rate started to decrease immediately after trapping began.

A source of photodamage consistent with our data is the production of excited-state (singlet) oxygen, mediated by a sensitizer molecule (Calmettes and Berns, 1983; Block, 1990; Svoboda and Block, 1994). Singlet oxygen is a long-lived, highly reactive species with well-established toxicity (Pryor, 1986; Dahl et al., 1987). While it is possible to produce singlet oxygen directly with laser illumination (Rosenthal, 1985), transitions from the ground state of molecular oxygen to the low-lying excited states are forbidden (Krupenie, 1972). Moreover, the absorption spectrum for molecular oxygen does not resemble the action spectrum for *E. coli*. Singlet oxygen may also be produced indirectly by exciting the triplet state of some sensitizer molecule, which in turn excites oxygen (Foote, 1976). It is conceivable, therefore, that the action spectrum for *E. coli* matches the spectrum of an unidentified sensitizer. This conjecture is consistent with the observed reduction in damage when oxygen is removed from the sample, and by the relationship between intensity and damage. The lack of a damage threshold and its linear time course suggests that the toxic species may have a short lifetime (a longer-lived species that accumulated would be expected to produce damage at a rate that increased with time). Other possibilities exist. For example, the absorbing species could itself directly damage cells, independent of oxygen per se, but be present in concentrations that depended indirectly on the oxygen tension.

This work was motivated, in part, by a search for the most favorable wavelength for optical trapping in biological work. Based on these data, some general conclusions can be reached concerning the design of optical tweezers. Spectral transmission characteristics suggest that microscope objectives designed for fluorescence are better suited to optical trapping work than the (more costly) highly corrected objectives designed for general high NA use. The large variation in throughput across the near-infrared portion of the spectrum means that careful consideration should be given to transmission characteristics before any objective for trapping work is selected. We also note that our measurements of transmission for most of the objectives tested differed from the test data supplied by various manufacturers, with our figures invariably being lower by 10–30%. This difference may be attributable to their use of integrating spheres to measure transmission through high-NA objectives, rather than the dual-objective method employed here. Integrating spheres do not distinguish between scattered and refracted light and therefore count scattered rays, which do not contribute usefully to trapping.

The action spectrum (Figs. 5 and 6) suggests that the region between 870 and 910 nm is particularly damaging and should be avoided, especially for work in vivo. The least harmful wavelengths are 830 and 970 nm, which are about a factor of 2 less destructive than the 1064 nm Nd:YAG wavelength in common use. Currently, single-mode diode lasers are available at all the favorable wavelengths, but only at relatively low power (typically, ~50–1000 mW). Continuing developments in diode laser technology may improve this situation, but there has been little increase in peak powers over the last 4 years. The fact that 970 nm is near the wavelength favored for pumping erbium fiber lasers in the communications industry (980 nm) augurs well for the development of economical, hybrid diode-based designs that may eventually reach higher powers.

The dramatic increase in lifetime promoted by the removal of oxygen suggests that where possible, scavengers or other means should be employed to reduce the oxygen tension in trapping experiments. While this strategy works well for in vitro protein assays and anaerobic organisms, it is obviously untenable for work with most eukaryotes. For the latter, a useful approach may involve adding quenchers of singlet oxygen to media. These include simple amino acids (e.g., histidine, methionine, or tryptophan) and powerful antioxidant compounds such as β-carotene, DABCO (diazabicyclo [2,2,2]octane), or α-tocopherol (vitamin E). The trapped-and-tethered cell assay presented here should provide a ready means for testing the protective potential of such compounds.

We thank Prof. Steven Lyon for generously providing lab space, equipment, and technical advice. We thank Prof. Howard Berg for the generous loan of the video cursor box, and Dr. Karen Fahrner for the generous gift of strain KAF95. We thank the Princeton University Department of Chemical Engineering teaching lab for the use of their incubator. We are indebted to Drs. Lisa Satterwhite, Koen Visscher, and Mark Schnitzer for helpful discussions, Jason Hsu for preliminary work on this project, Anja Brau for assistance with the anaerobic data collection, and Jeff Lehrman for assistance with LabView programming. We thank Neil Barlow of Micron Optics for the loan of Nikon microscope objectives and Geoff Daniels of Leica America for the loan of Leica objectives for transmission measurements.

KCN was supported by a training grant from the National Institutes of Health. SMB acknowledges support from grants from the National Science Foundation, the National Institutes of Health, and the W. M. Keck Foundation.

REFERENCES

Ashkin, A. 1974. Trapping of atoms by resonance radiation pressure. *Appl. Phys. Lett.* 19:283–285.

Ashkin, A., J. M. Dziedzic, J. E. Bjorkholm, and S. Chu. 1986. Observation of a single beam gradient force optical trap for dielectric particles. *Opt. Lett.* 11:288–290.

Ashkin, A., and J. M. Dziedzic. 1989. Optical trapping and manipulation of single living cells using infra-red laser beams. *Ber. Bunsenges. Phys. Chem.* 93:254–260.

Ashkin, A., J. M. Dziedzic, and T. Yamane. 1987. Optical trapping and manipulation of single cells using infrared laser beams. *Nature.* 330: 769–771.

Berg, H. C., and L. Turner. 1993. Torque generated by the flagellar motor of *Escherichia coli*. *Biophys. J.* 65:2201–2216.

Berns, M. W. 1976. A possible two-photon effect in vitro using a focused laser beam. *Biophys. J.* 16:973–977.

Block, S. M. 1990. Optical tweezers: a new tool for biophysics. *In* Noninvasive Techniques in Cell Biology. Modern Review of Cell Biology, Vol. 9. J. K. Foskett and S. Grinstein, editors. Wiley-Liss, New York. 375–402.

Block, S. M., and H. C. Berg. 1984. Successive incorporation of force-generating units in the bacterial rotary motor. *Nature.* 309:470–472.

Block, S. M., D. F. Blair, and H. C. Berg. 1989. Compliance of bacterial flagella measured with optical tweezers. *Nature.* 338:514–518.

Block, S. M., J. E. Segall, and H. C. Berg. 1982. Impulse responses in bacterial chemotaxis. *Cell.* 31:215–226.

Block, S. M., J. E. Segall, and H. C. Berg. 1983. Adaptation kinetics in bacterial chemotaxis. *J. Bacteriol.* 154:312–323.

Bushanam, G. S., and F. S. Barnes. 1975. Laser-generated thermoelastic shock wave in liquids. *J. Appl. Phys.* 46:2074–2082.

Calmettes, P. P., and M. W. Berns. 1983. Laser induced multiphoton processes in living cells. *Proc. Natl. Acad. Sci. USA.* 80:7197–7199.

Dahl, T. A., R. A. Midden, and P. E. Hartman. 1987. Pure singlet oxygen cytotoxicity for bacteria. *Photochem. Photobiol.* 46:345–352.

Foote, C. S. 1976. Photosensitized oxidation and singlet oxygen: consequences in biological systems. *In* Free Radicals in Biology, Vol. II. W. A. Pryor, editor. Academic Press, New York. 85–133.

Hu, C. 1969. Spherical model of an acoustical wave generated by rapid laser heating in a liquid. *J. Acoust. Soc. Am.* 46:728–735.

König, K., H. Liang, M. W. Berns, and B. J. Tromberg. 1995. Cell damage by near-IR microbeams. *Nature.* 377:20–21.

König, K., H. Liang, M. W. Berns, and B. J. Tromberg. 1996a. Cell damage in near-infrared multimode optical traps as a result of multiphoton absorption. *Opt. Lett.* 21:1090–1092.

König, K., Y. Tadir, P. Patrizio, M. W. Berns, and B. J. Tromberg. 1996b. Effects of ultraviolet exposure and near infrared laser tweezers on human spermatozoa. *Hum. Reprod.* 11:2162–2164.

Krupenie, P. H. 1972. The spectrum of molecular oxygen. *J. Phys. Chem. Ref. Data.* 1:423–520.

Kuwajima, G. 1988. Construction of a minimum-size functional flagellin of *Escherichia coli*. *J. Bacteriol.* 170:3305–3309.

Liang, H., K. T. Vu, P. Krishnan, T. C. Trang, D. Shin, S. Kimel, and M. W. Berns. 1996. Wavelength dependence of cell cloning efficiency after optical trapping. *Biophys. J.* 70:1529–1533.

Liu, Y., D. K. Cheng, G. J. Sonek, M. W. Berns, C. F. Chapman, and B. J. Tromberg. 1995a. Evidence for localized cell heating induced by infrared optical tweezers. *Biophys. J.* 68:2137–2144.

Liu, Y., G. J. Sonek, M. W. Berns, K. König, and B. J. Tromberg. 1995b. Two-photon fluorescence excitation in continuous-wave infrared optical tweezers. *Opt. Lett.* 20:2246–2248.

Liu, Y., G. J. Sonek, M. W. Berns, and B. J. Tromberg. 1996. Physiological monitoring of optically trapped cells: assessing the effects of confinement by 1064-nm laser tweezers using microfluorometry. *Biophys. J.* 71:2158–2167.

Lustmann, J., M. Ulmansky, A. Fuxbrunner, and A. Lewis. 1992. Photoacoustic injury and bone healing following 193 nm excimer laser ablation. *Lasers Surg. Med.* 12:390–396.

Manson, M. D., P. M. Tedesco, and H. C. Berg. 1980. Energetics of flagellar rotation in bacteria. *J. Mol. Biol.* 138:541–561.

Misawa, H., M. Koshioka, K. Sasak, N. Kitamura, and H. Masuhara. 1991. Three dimensional optical trapping and laser ablation of a single polymer latex in water. *J. Appl. Phys.* 70:3829–3836.

Palmer, K. F., and D. Williams. 1974. Optical properties of water in the near infrared. *J. Opt. Soc. Am.* 64:1107–1110.

Parkinson, J. S. 1978. Complementation analysis and deletion mapping of *Escherichia coli* mutants defective in chemotaxis. *J. Bacteriol.* 135: 45–53.

Parkinson, J. S., S. R. Parker, P. B. Talbert, and S. E. Houts. 1983. Interactions between chemotaxis genes and flagellar genes in *Escherichia coli*. *J. Bacteriol.* 155:265–274.

Patel, C. K. N., and A. C. Tam. 1981. Pulsed optoacoustic spectroscopy of condensed matter. *Rev. Mod. Phys.* 53:517–550.

Pryor, W. A. 1986. Oxy-radicals and related species: their formation, lifetimes, and reactions. *Annu. Rev. Physiol.* 48:657–667.

Rosenthal, I. 1985. Chemical and physical sources of singlet oxygen. *In* Singlet O_2, Vol. I, Physical and Chemical Aspects. A. A. Frimer, editor. CRC Press, Boca Raton, FL. 13–38.

Svoboda, K., and S. M. Block. 1994. Biological applications of optical forces. *Annu. Rev. Biomol. Struct.* 23:247–285.

Vorobjev, I. A., H. Liang, W. H. Wright, and M. W. Berns. 1993. Optical trapping for chromosome manipulation: a wavelength dependence of induced chromosome bridges. *Biophys. J.* 64:533–538.

Yashima, Y., D. J. McAuliffe, and T. J. Flotte. 1990. Cell selectivity laser induced photoacoustic injury of skin. *Lasers Surg. Med.* 10:280–283.

Yashima, Y., D. J. McAuliffe, S. L. Jacques, and T. J. Flotte. 1991. Laser-induced photoacoustic injury of skin: effect of inertial confinement. *Lasers Surg. Med.* 11:62–68.